frontiers | Frontiers in Earth Science

TYPE Original Research
PUBLISHED 29 August 2025
DOI 10.3389/feart.2025.1671000

OPEN ACCESS

EDITED BY
Qingchao Li,
Henan Polytechnic University, China

REVIEWED BY
Wei Li,
Northeast Petroleum University, China
Sunhua Deng,
Jilin University of the Arts, China
Yulin Ma,
Liaoning Technical University, China

*CORRESPONDENCE
Xiao Li,
2023310265@link.tyut.edu.cn,
xiaoli6@cnooc.com.cn

RECEIVED 22 July 2025
ACCEPTED 14 August 2025
PUBLISHED 29 August 2025

CITATION
Li X, Tang Y, Li Y, Yang F, Wu X, Sun J, Cui J, Zhang Q, Yuan S and Kang Z (2025) Study on pyrolysis characteristics of oil-rich coal under *in-situ* conditions and industrial-scale extraction simulation.
Front. Earth Sci. 13:1671000.
doi: 10.3389/feart.2025.1671000

Study on pyrolysis characteristics of oil-rich coal under *in-situ* conditions and industrial-scale extraction simulation

Xiao Li[1,2]*, Ying Tang[1,2], Youwu Li[1,2], Fan Yang[1,2], Xiaodan Wu[1,2], Jingyao Sun[1,2], Jingyun Cui[1,2], Qing Zhang[1,2], Siqi Yuan[1,2] and ZhiQin Kang[3]

[1]CNOOC Key Laboratory of Liquefied Natural Gas and Low-carbon Technology, Beijing, China, [2]CNOOC Gas & Power Group, Research & Development Center, Beijing, China, [3]Taiyuan University of Technology, Taiyuan, China

Introduction: *In-situ* pyrolysis technology for oil-rich coal represents a low-carbon resource development strategy characterized by 'hydrogen extraction and carbon retention,' holding significant importance for advancing the efficient exploitation of coal-based oil and gas resources. However, substantial differences exist between *in-situ* pyrolysis and conventional pyrolysis in terms of conversion efficiency and product composition, making the control of operating conditions a critical challenge in this field.

Methods: This study utilized large-sized block oil-rich coal samples from the Xie Gou mining area in Shanxi Province. Employing a self-developed, fully enclosed pyrolysis experimental system, the research simulated the high-temperature, high-pressure, slow-heating-rate, and long-duration reaction environment typical of *in-situ* pyrolysis. The distribution patterns of gaseous, liquid, and solid pyrolysis products from the oil-rich coal under varying temperatures were systematically investigated. Building upon the experimental results, industrial-scale simulations of oil-rich coal *in-situ* pyrolysis were conducted using COMSOL Multiphysics software.

Results and Discussion: The key findings are as follows: (1) The primary gaseous product of the pyrolysis reaction is CH_4, with the total gas yield increasing significantly as temperature rises; (2) The temperature window of 450 °C–550 °C offers the potential for maximizing light oil recovery; (3) The stability of the carbon skeleton within the oil-rich coal enhances progressively as the pyrolysis reaction proceeds; (4) For industrial application, optimal oil production is achieved within approximately 500 days of heating, while optimal gas production occurs around 1900 days of heating. This study provides crucial theoretical support for the industrialization of oil-rich coal *in-situ* pyrolysis and demonstrates considerable application potential for the extraction of high-value oil and gas fuels.

KEYWORDS

***in-situ* pyrolysis, three-phase products, oil-rich coal, closed system, numerical simulation**

1 Introduction

In recent years, with the intensification of global extreme weather events, world-wide emphasis on climate governance has significantly increased. As one of the world's major economies, China has correspondingly proposed its 'carbon peak and carbon neutrality' targets. However, given that coal occupies the dominant position in China's energy consumption structure—a situation expected to persist long-term—the development and utilization of oil-rich coal is urgently required to address the energy reality characterized by 'abundant coal but scarce oil and gas.' As a special coal resource possessing triple attributes of coal, oil, and gas (Feng et al., 2016; Kang et al., 2020), oil-rich coal features high hydrogen content and abundant aliphatic structures (Wang S. et al., 2024). Through pyrolysis, it can yield 7%–12% coal tar, enabling the efficient utilization of coalbased oil and gas resources (Wang M. et al., 2024; Wang et al., 2021; Ning et al., 2025). China's reserves of oil-rich coal exceed 550 billion tonnes (5.5×10^{11}t), with potential oil and gas resources estimated at 50 billion tonnes and 75 trillion cubic meters, respectively, indicating immense resource potential (Ju et al., 2021).

Numerous scholars domestically and internationally have conducted research on oil-rich coal development and utilization technologies. Investigations into the thermal decomposition characteristics of oil-rich coal form the theoretical foundation for its utilization. Yang et al. (2023a) analyzed the pyrolysis characteristics of oil-rich coal within its original geological environment, determining its typical thermodynamic functions and related parameters, and established the primary reaction functions for the oil-rich coal pyrolysis process. Bhattacharyya et al. (2024) examined the product composition of biomass-containing coal samples under various pyrolysis conditions, identifying the influence of biomass component content and pyrolysis conditions on the pyrolysis products. Zhang et al. (2025) systematically studied the structural characteristics of oil-rich coal and their correlation with pyrolysis products through proximate and ultimate analysis, providing a theoretical basis for the precise directional conversion of oil and gas. Fu et al. (2023a) employed techniques like electrical heating to pyrolyze oil-rich coal after artificial fracturing, investigating the optimal pyrolysis temperature windows under different coal quality characteristics and pyrolysis atmospheres. Ye et al. (2023) focused on analyzing heat transfer modes and physicochemical reactions during pyrolysis within fractured porous zones of oil-rich coal. Thermogravimetric analysis (TGA) is the most frequently used method for studying oil-rich coal pyrolysis characteristics. Guo et al. (2023) analyzed the distribution characteristics of oil and gas resources in recoverable strata and their impact on recovery efficiency by studying the properties of residual organic matter postpyrolysis. To analyze the differences between oil-rich coal and ordinary coal, Yu et al. (2023) utilized TGA coupled with *in-situ* Fourier transform infrared spectroscopy (FTIR) to study the pyrolysis characteristics of oil-rich coal macerals. They discovered that the vitrinite in oil-rich coal possesses more aliphatic long chains and alkyl side chains compared to ordinary coal, resulting in superior py-rolysis reactivity. Xie et al. (2018), building on this, further analyzed the differences in the decomposition behavior of carboxylic acid groups between oil-rich coal and ordinary bituminous coal during the pyrolysis process by using infrared spectroscopy technology. Yu G. et al. (2024) characterized the low-temperature pyrolysis processes of three coal types using TGA, deriving the various product yields from oil-rich coal pyrolysis by analyzing its reaction process parameters. Furthermore, many scholars have investigated practical engineering application technologies for oil-rich coal pyrolysis. Chen M. et al. (2025) simulated the influence of temperature, pressure, and other factors on the *in-situ* pyrolysis reaction process by conducting gas pressurization experiments on oil-rich coal in autoclaves. Duan et al. (2024) conducted field pyrolysis experiments on oil-rich coal in Northern Shaanxi, China, comprehensively analyzing suitable geological conditions for *in-situ* pyrolysis and obtaining optimal parameters such as formation temperature and pressure. Krumm et al. (2017) enhanced oil and gas recovery from coal seams by injecting CO_2 after heating deep coal layers, observing changes in coal structure and gas adsorption capacity with increasing heating temperature. Wang et al. (2025a), Wang L. et al. (2024), and Wang et al. (2025b) conducted extensive experimental studies on the pyrolysis product distribution, anisotropic evolution, and heat transfer mechanisms of coal samples under high-temperature steam environments, providing theoretical foundations for investigating both macroscopic and microscopic mechanisms of coal pyrolysis. Extensive research on *in-situ* pyrolysis of oil-rich coal indicates that, compared to traditional surface retorting processes, this technology offers advantages such as reduced carbon emissions, minimized surface disturbance, and improved energy recovery efficiency (Yuan et al., 2025; Ju et al., 2022; Tian et al., 2024; Yu Z. et al., 2024; Dong et al., 2025).

Although numerous scholars have investigated the pyrolysis mechanism of oil-rich coal and *in-situ* pyrolysis technologies, research to date has predominantly focused on rapid surface pyrolysis of powdered coal samples. Studies on the pyrolysis processes and characteristics of largescale oil-rich coal under prolonged, enclosed *in-situ* conditions remain extremely scarce. Building upon this gap, this research employs lump oil-rich coal from the Xie Gou Mine in Lvliang, Shanxi Province as the study object. Integrating gas chromatography-mass spectrometry (GC-MS) and rock thermal analysis technology, the study simulates the reaction processes of large coal masses under extended duration and controlled low heating rates, along with parameter variations induced by high-temperature and high-pressure conditions. It systematically analyzes the influence of pyrolysis temperature on the three-phase products of oil-rich coal. Based on experimental parameter fitting, numerical simulations of hundred-meter-scale oil-rich coal *in-situ* pyrolysis were conducted using COMSOL Multiphysics software. This work provides both theoretical support and technical exploration for the industrialization of oil-rich coal *in-situ* pyrolysis.

2 Materials and methods

2.1 Sample preparation

The experimental coal samples were selected from oil-rich coal at the Xie Gou Mine in Shanxi Province, China. The Xiegou coal samples employed in this study are representative of 78.3% of Shanxi Province's oil-rich coal reserves. The selected samples exhibited

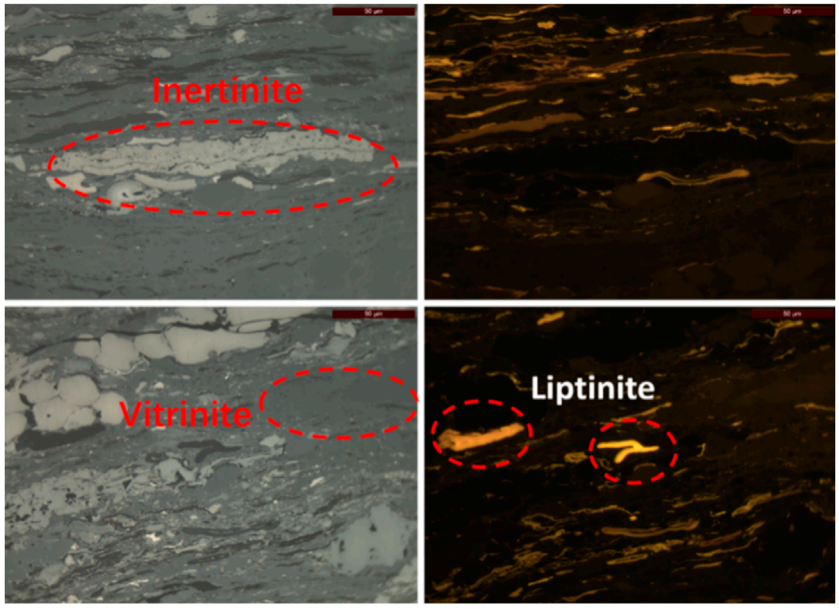

FIGURE 1
Microscopic component identification of whole rock thin Section (1:500).

TABLE 1 Gieseler distillation product distribution and $R_{o,max}$ of Xiegou gas coal.

Water/%	Gases/%	Oil/%	Char/%	Ro max/%
7.15	6.5	9.95	76.45	0.74

black, lumpy morphology with dense texture and weak greasy luster. After crushing and sieving to obtain 20–30 mm particle size fractions, the coal was dried at 105 °C for 24 h to remove surface moisture. The mean maximum vitrinite reflectance ($R_{o,max}$) of the prepared samples was measured as 0.74% ± 0.02. Organic maceral composition was determined using a Leica DM6000M image analyzer employing a grayscale-reflectance model and automated vitrinite recognition technology (see Figure 1), yielding the following composition: vitrinite (60.3%), inertinite (30.1%), and liptinite (10.6%). Gray-King assay pyrolysis was conducted under conditions of 600 °C final temperature, 5 °C/min heating rate, and 15-min holding time, with resultant pyrolysis products detailed in Table 1.

Under the conditions of an initial temperature of 25 °C, a final temperature of 900 °C, and air as the carrier gas, the weight loss rate of oil-rich coal was measured at a heating rate of 10 °C/min. The results are shown in Figure 2, and the sample exhibited a relatively high weight loss rate.

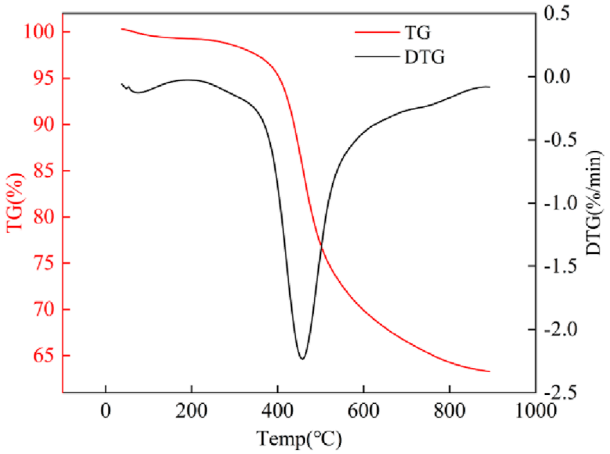

FIGURE 2
Thermogravimetric curve of Xiegou Oil-rich coal.

2.2 Pyrolysis experiment

Fifty grams coal samples were reacted in a high-temperature/high-pressure autoclave to simulate *in-situ* pyrolysis of oil-rich coal under varying thermal conditions. Six separate samples underwent sealed pyrolysis experiments at designated temperatures of 350 °C, 400 °C, 450 °C, 500 °C, 550 °C, and 600 °C. Detailed data are shown in Table 2.

The experiments in this study were conducted to simulate the *in-situ* underground environment, and a reaction system was constructed to simulate the *in-situ* temperature-pressure conditions of the strata over extended periods (schematic diagram of the equipment shown in Figure 3, equipment photos shown in Figure 4). The system consists of four main components: the data acquisition and control module; the *in-situ* pyrolysis module, which provides a sealed reaction environment with a maximum pressure of 50 MPa; the product separation and collection module; and the precise atmosphere control module.

TABLE 2 Final stable pressure of *in-situ*pyrolysis tar-rich coal system.

Temperature/°C	350	400	450	500	550	600
Pressure/MPa	0.8	4.3	7.2	9.3	11.7	14.5

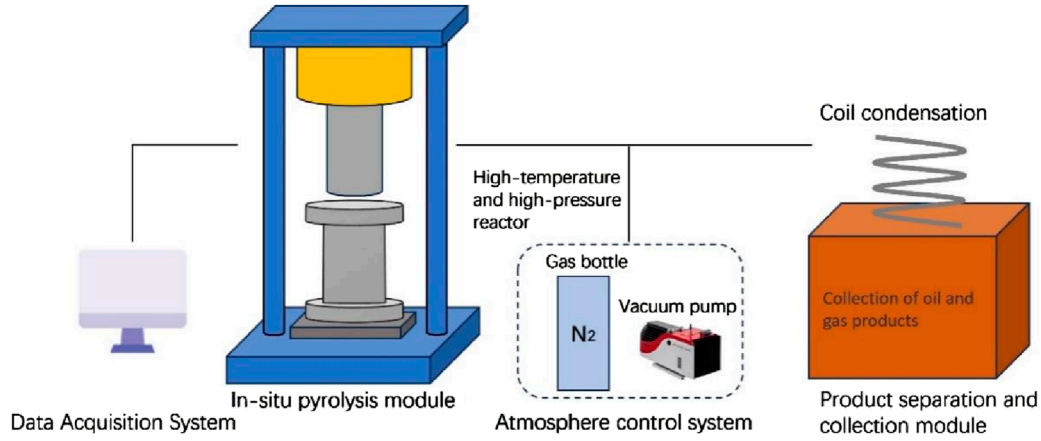

FIGURE 3
Schematic of long-term in-situ temperature-pressure simulation systems.

FIGURE 4
Long-term in-situ temperature-pressure simulation reaction system.

During the experiment, the pretreated samples were placed in the reaction vessel, and a 15 MPa axial load was applied using a servo pressurization system to simulate the *in-situ* stress conditions at a depth of approximately 600 m underground. The system was then thoroughly checked for airtightness, followed by a 1 h vacuum pretreatment to eliminate any residual gas interference.

In the experiment, each sample was heated to the preset final pyrolysis temperature at a heating rate of 1 °C min^{-1}. To investigate the distribution of pyrolysis products under long-term closed conditions, the reactor was completely sealed immediately after heating commenced, and the reaction was maintained at the final temperature. Under these conditions, the pressure inside the reactor gradually increased over time. Heating was ceased after the pressure remained stable without increasing for 2 h, with 48 h ultimately determined as the duration for a single experiment. Following the experiment, once the system cooled to 180 °C, the outlet of the high-temperature and high-pressure reactor was opened. Volatile products generated by pyrolysis entered the product separation system, where oil-gas products and solid residues were collected. The reactor and pipelines were then flushed with dichloromethane. The oil phase in the high-pressure reactor and pipelines was labeled as "discharged oil," while the oil phase in the residual solid was obtained via extraction and labeled as "residual oil."

After long-term reaction under *in situ* conditions, the morphology of the coal sample underwent significant changes: the originally dispersed coal particles coked and agglomerated together, thereby affecting the heat and mass transfer efficiency, as shown in Figure 5.

2.3 Theoretical basis for industrial-scale extraction simulation of oil-rich coal

2.3.1 Physical model

The well layout for electric heating exploitation of oil-rich coal is shown in Figure 6. To ensure the model conforms to actual conditions, the total size of the model is a cuboid of 50 × 50 × 30 m, and an axial pressure of 15 MPa was applied to simulate the oil-rich coal reservoir with a burial depth of 600 m. A 6-m-thick oil-rich coal seam is positioned in the middle of the model; this coal seam is enclosed by two layers (roof and floor), each 12 m thick, as depicted in Figure 6a. Figure 6b illustrates the layout of heaters and production wells, where red represents heaters and blue represents production wells. The outer-most heaters are located 7 m from the boundary. Heaters are arranged at 3-m intervals, with a production well placed midway between every two adjacent heaters:

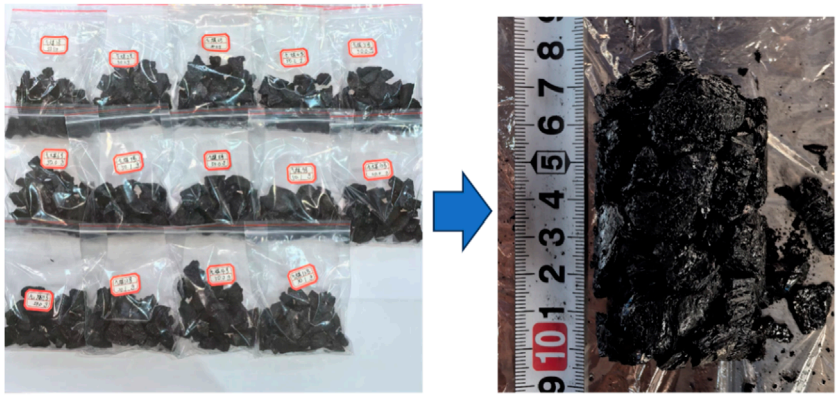

FIGURE 5
Photos of Xiegou tar-rich coal before and after pyrolysis. **(a)** Initial sample. **(b)** Post-pyrolysis sample.

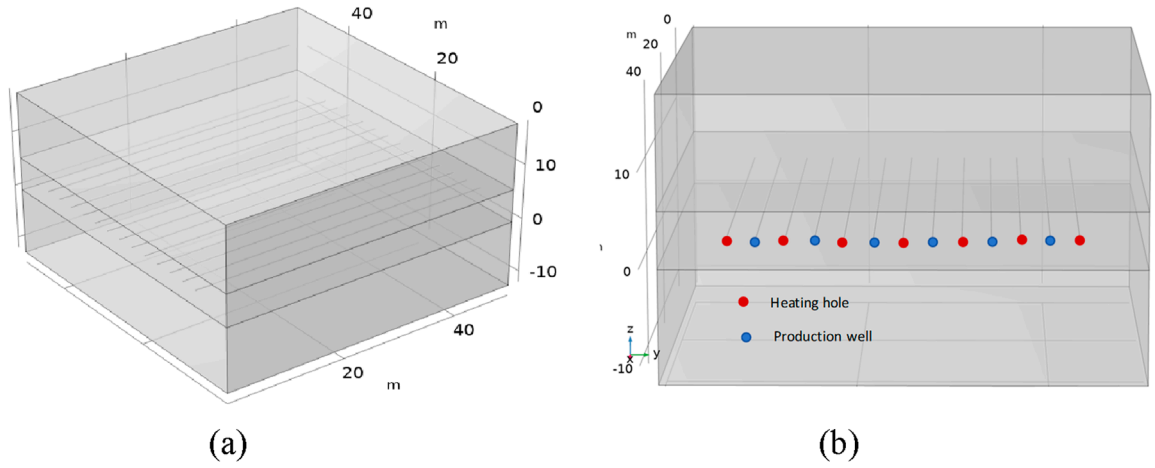

FIGURE 6
Simulation physical model for oil-rich coal mining. **(a)** Front view. **(b)** Pattern shape.

2.3.2 Mathematical model

2.3.2.1 Energy conservation equation

$$(1-\phi)\rho_r C_{pr}\frac{\partial T_r}{\partial t} = \lambda_r T_{r,ii} + W_s$$

Where: ϕ is the porosity of oil-rich coal; ρ_r is the density of oil-rich coal; C_{pr} is the heat capacity of oil-rich coal; T_r is the temperature of oil-rich coal; λ_r is the thermal conductivity of oil-rich coal; W_s is the heat source term for rock thermal conduction (Kou et al., 2023; Chen Z. et al., 2025).

2.3.2.2 Gas energy conservation equation

$$C_{pg}\frac{\partial(\rho_g T_g)}{\partial t} = \lambda_g T_{g,ii} - C_{pg}\left(\rho_g k_i p_{g,i} T_g\right)_{,i} + W_g$$

Where: C_{pg} is the heat capacity of the mixed gas; ρ_g is the density of the mixed gas; T_g is the temperature of the mixed gas; k_i is the permeability of oil-rich coal in the i direction; λ_g is the thermal conductivity of oil-rich coal; W_g is the heat source term for fluid heat transfer; ρ_g is the pressure of the mixed gas (Chen et al., 2024; Yang et al., 2023b).

2.3.2.3 Static equilibrium equation

$$(\lambda(T_r)+\mu(T_r))u_{j,ji} + \mu(T_r)\mu_{i,jj} + F_i - \beta_T T_{r,i} - \alpha p_{g,i} = 0$$

Where: $(\lambda(T_r), \mu(T_r)$ are both Lamé constants; u is the displacement; β_T is the thermal expansion coefficient of oil-rich coal; α is the Biot coefficient; F_i is the volume stress; $p_{g,i}$ is the pressure of the mixed gas; T_r is the temperature of the oil shale formation (Wu et al., 2022; Wang et al., 2019).

2.3.3 Experimental parameter fitting model

During the pyrolysis process, the permeability, thermal conductivity, and thermal expansion coefficient of the oil-rich coal

reservoir all vary with temperature, which were fitted based on the data obtained from experimental studies to obtain the relational expressions for each parameter of the physical model. In addition, considering that the temperature range in the numerical simulation process is larger than that in the experiments, the permeability within the temperature range beyond the experimental range is still extrapolated horizontally based on adjacent experimental data. Since oil-rich coal is a weakly anisotropic material (Yang et al., 2021), the coal seam is assumed to be an isotropic reservoir.

2.3.3.1 The variation law of permeability with temperature

The fitting equation of coal seam permeability varying with temperature is:

$$\begin{cases} k_{(0<T\leq 300)} = \left(0.01996 - 0.00259 * x + 7.87059E - 5 * x^2 - 2.33795E - 7 * x^3\right) \\ k_{(300<T\leq 650)} = \left(821.7911 + \dfrac{1.72074 - 821.7911}{1 + exp\left(\frac{x-529.54378}{19.57922}\right)}\right) \end{cases}$$

Where: $k_{(0<T\leq 300)}$ is the permeability of the coal seam when the temperature is greater than 0 °C and less than or equal to 300 °C, mD; $k_{(300<T\leq 650)}$ is the permeability of the coal seam when the temperature is greater than 300 °C and less than 650 °C, mD; x is the temperature, °C.

2.3.3.2 The variation law of the coefficient of thermal expansion with temperature

In previous experiments, we employed a Netzsch dilatometer to measure the thermal expansion coefficient of coal under varying temperatures and pressures. The thermal expansion coefficient equation is as follows:

$$\begin{cases} \alpha = 0.014T - 1.005 \\ \alpha = 0.017T + 1.423 \end{cases}$$

Where: α is the coefficient of thermal expansion, 1/°C; T represents temperature, °C.

2.3.3.3 The variation law of thermal conductivity coefficient at temperature

There is a critically important relationship between thermal conductivity and the heat transfer characteristics of oil-rich coal seams. In the author's previous research, the thermal conductivity of oil-rich coal was fitted and obtained using the NETZSCH LFA 457 laser thermal conductivity analyzer:

$$\lambda = 0.07127 + \frac{0.58072}{1 + e^{\frac{(T-347.123)}{dx}}}$$

Where: λ is the thermal conductivity coefficient of oil-rich coal, W/(m·K) (Wang and Feng, 2021);

2.3.4 Boundary conditions

Boundary conditions for the temperature field: The initial temperature of the coal seam, roof, and floor is 20 °C; the temperature of heating wells is fixed at 600 °C; the initial temperature of production wells is 20 °C; and the surrounding boundaries of the model are thermally insulated.

Boundary conditions for the solid deformation field: The upper boundary is subject to a vertically downward boundary load of 15 MPa to simulate the environment at a burial depth of 600 m; the surrounding boundaries are roller supports to constrain horizontal displacement; and the lower boundary is a fixed boundary.

3 Experimental results

3.1 *In-situ* pyrolysis gas-phase product analysis

Through sealed pyrolysis experiments on oil-rich coal samples from Shanxi Xie Gou Mine, the total gas yield and system pressure under heating conditions were measured. The temperature-dependent correlations are plotted in Figure 7. As shown, when temperature increased from 350 °C to 600 °C, system pressure rose from 0.8 MPa to 14.5 MPa. Analysis of gas yield reveals a progressive increase to 150 mL/g with rising temperature, exhibiting a growth rate that initially accelerates then decelerates.

Figure 8a shows the variation diagram of the proportion of each component in the pyrolysis gases with temperature, from the figure it can be seen that at 350 °C, CO_2 accounts for the highest proportion in the gaseous products, with increasing temperature the proportion of CO_2 gradually decreases, and the proportion also gradually decreases, at 500 °C a slight rebound occurs; the proportion of CH_4 gas rapidly increases with increasing temperature, although a significant decrease appears in the temperature range of 450 °C–500 °C, thereafter it rapidly increases, reaching a peak of 82.1% at 550 °C; the proportions of C_2 and C_3 gases increase in the range of 350 °C–400 °C, reaching peaks at 400 °C, afterwards with increasing temperature the proportions of both gases decrease; furthermore, the proportion of H_2 overall shows a decreasing trend, but exhibits a slight rebound at 600 °C, in contrast, throughout the entire pyrolysis reaction process the proportion of CO remains relatively small.

Figure 8b shows the temperature-dependent yield trends of pyrolytic gas components. CH_4 yield exhibits the most significant increase, reaching 113.2 mL/g at 600 °C. Conversely, CO, C_2, and C_3 yields decline progressively with rising temperature, aligning with their proportional composition trends. Within the 550 °C–600 °C interval, CH_4 and H_2 yields increase while CO_2 yield remains comparable to 500 °C levels.

3.2 *In-situ* pyrolysis liquid-phase products analysis

Figure 9 illustrates variations in residual and discharged oil yields after prolonged sealed pyrolysis of oil-rich coal. As shown in Figure 9, discharged oil yield gradually increases between 350 °C and 450 °C but declines with further temperature rise. Additionally, residual oil yield progressively decreases with increasing temperature. When temperature continues rising to 450 °C, discharged oil yield increases; after this point, both discharged and residual oils show decreasing trends.

Figure 10 shows compositional changes in discharged and residual oils from sealed pyrolysis of lump oil-rich coal. Using SARA analysis, coal tar is categorized into aromatics, saturates, asphaltenes, and non-hydrocarbons. Observing Figure 10, under prolonged *in-situ* sealed pyrolysis conditions: with increasing temperature, saturates content in discharged oil shows an overall rising trend, while in residual oil, saturates content exhibits a more pronounced increase from 350 °C to 600 °C; while aromatics content remains relatively high in both oil types; additionally, non-hydrocarbons show minimal fluctuations between 350 °C and 600 °C, with

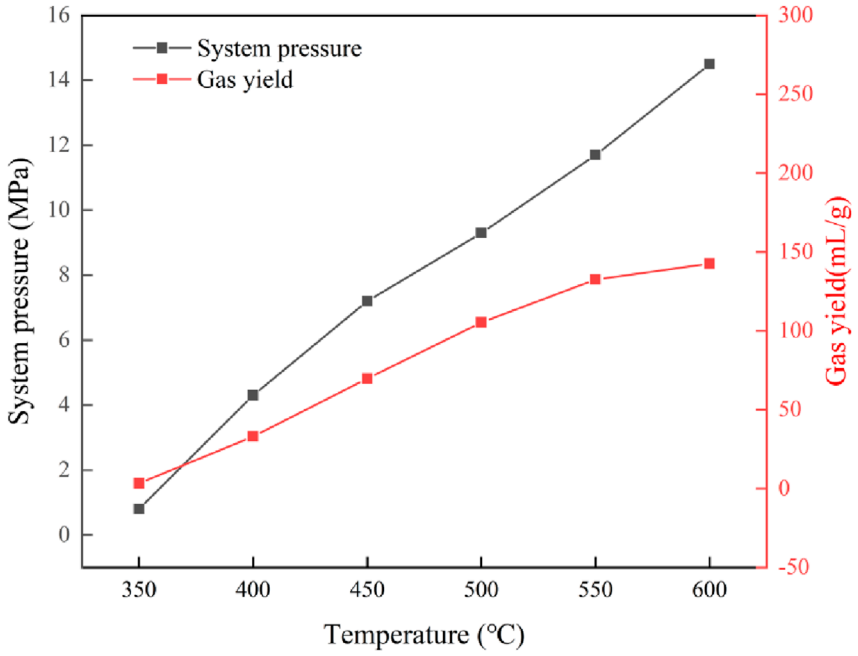

FIGURE 7
Pressure in a closed system and pyrolysis gas yield.

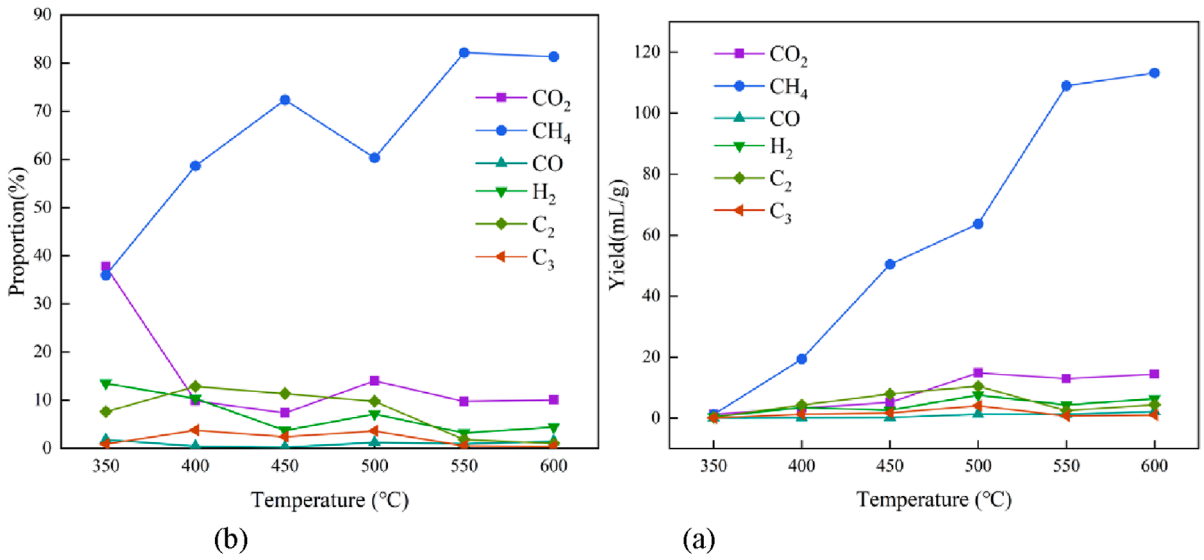

FIGURE 8
Pyrolysis gas composition and yield distribution. **(a)** Yield of pyrolysis gas. **(b)** Proportion of pyrolysis gas.

discharged oil maintaining greater stability at approximately 20%; asphaltenes content decreases in both discharged and residual oils.

Figure 11 shows the carbon number distributions of discharged and residual oils from prolonged sealed pyrolysis of lump oil-rich coal. According to GC-MS analysis, the carbon number distributions of discharged and residual oils exhibit similar trends with temperature change. Here, C_5–C_{16} components are defined as light fractions, C_{17}–C_{19} as medium fractions, and C_{20}^+ as heavy fractions. Based on Figure 11, as temperature increases, the light fraction content in discharged oil gradually rises, reaches a peak of 30.0% during 500 °C–550 °C, then declines after 550 °C. The light fraction content in residual oil also increases significantly but reaches its peak at 450 °C. C_{17}–C_{19} content in discharged oil remains stable between 17% and 25% without significant change, while in residual oil it increases significantly at 400 °C and stabilizes around 30% when temperature exceeds 400 °C; for heavy fractions (C_{20}^+),

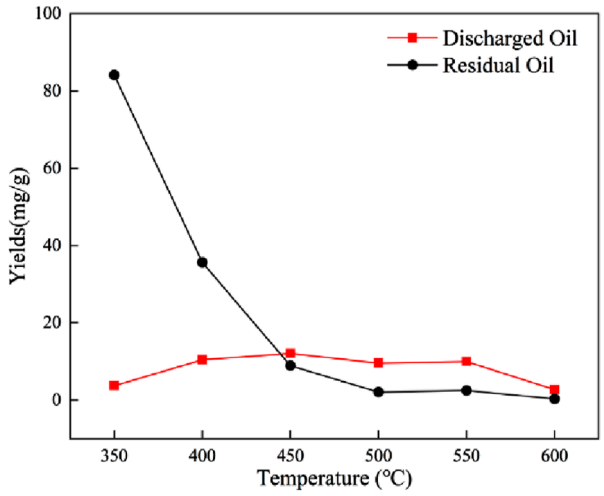

FIGURE 9
Residual and discharged oil yield vs. temperature curve.

both discharged and residual oils show an initial decrease followed by an increase trend: discharged oil decreases significantly from 350 °C to 550 °C to 49.2%, then rises to 72.3% at 600 °C, while residual oil decreases to 42.4% before rising with further temperature increase.

Comprehensive hydrocarbon chromatography studies indicate that within the 450 °C–550 °C temperature range, discharged oil exhibits higher proportions of light fractions and lower heavy fraction content; group component analysis further reveals elevated saturates content in discharged oil during this same interval.

3.3 *In-situ* pyrolysis solid products analysis

Analysis of solid residues from sealed pyrolysis of Xie Gou oil-rich coal using Rock-Eval pyrolysis equipment is presented in Figure 12. The original sample contains 69.19% TOC and 14.81% PC. With increasing temperature, TOC content continuously rises by 17.5%, while PC content decreases from 14.81% to 1.66%. Figure 12 further shows PC content decreases continuously with rising temperature, exhibiting particularly pronounced changes at 350 °C.

3.4 Analysis of simulation results obtained based on experimental data

3.4.1 Temperature field variation of in-situ pyrolysis via electric heating method

From the results of oil-rich coal pyrolysis experiments, it is known that when the temperature exceeds 350 °C, pyrolysis gas and coal tar start to generate in oil-rich coal. As the temperature increases, when the temperature exceeds 500 °C, the gas yield starts to increase while the oil yield decreases. Therefore, temperature is an important factor affecting the pyrolysis oil and gas yields of oil-rich coal, and also an important indicator reflecting the *in-situ* heating efficiency of oil-rich coal.

Figure 13 shows the variation law of the temperature field under different heating times, obtained by fitting experimental data. At 100 days, the temperature around the heaters rises, forming a pyrolysis zone, and the area with temperature above 500 °C accounts for 11.5% of the entire coal seam. As the heating time extends to 600 days, the high-temperature area continues to expand to the distal end of the heaters; at this time, the 500 °C isotherms are still not interconnected, and the area above 500 °C accounts for 40.6% of the entire coal seam.

When the heating time reaches 1,000 days, the 500 °C isotherms gradually interconnect. At 1,500 days, the temperature of the coal seam between heaters has all reached above 500 °C, with the average temperature of the coal seam reaching 502.1 °C. This indicates that the *in-situ* electric heating method can effectively heat the oil-rich coal seam, thereby exploiting oil and gas resources.

3.4.2 Yield variation of three-phase products of in-situ pyrolysis via electric heating method

Based on the yield data obtained from experiments, the cumulative yields of discharged oil, CH_4, and H_2 from *in-situ* pyrolysis of oil-rich coal at the industrial scale were derived, as shown in Figure 14. The cumulative yields of liquid fuel and natural gas both continuously increase with heating time, but the growth rate gradually slows down, reflecting the gradual nature of the pyrolysis reaction. Specifically, the cumulative yield of discharged oil increases from an initial 48,099 kg to a final 919,910 kg; CH_4 increases from 9.48×10^5 L to 3.23×10^7 L; and H_2 increases from 7.86×10^4 L to 2.37×10^6 L. The yields follow the order: CH_4 > discharged oil > H_2, with significant differences in their scales, consistent with the trends observed in previous experiments.

Discharged oil daily production change presents a pattern of first rapid rise then continuous decline: at 200 days reaching peak 2,320 kg, afterward sharply decreasing, after 400 days below 600 kg, after 1,500 days only less than 100 kg, indicating tar generation concentrates in the early low-medium temperature stage; CH_4 daily production peak (3.16×104 L) appears at 1,100 d, H_2 daily production peak appears at 1,900 d, its occurrence time latest, simultaneously daily production lowest, peak only 2,680 L.

4 Discussion

The oil-rich coal sample undergoes significant temperature-dependent changes in gaseous products, liquid products, and residual solids during thermal decomposition in a confined environment. Firstly, for pyrolytic gaseous products: the variation trends of total gas yield and system pressure show a distinct positive correlation with temperature, because elevated temperature promotes coal pyrolysis reactions, releasing more volatile organic compounds from the coal sample and converting them into gaseous products. Thus, the gas generation rate accelerates, increasing gas production. However, when temperature reaches 550 °C, high pressure in the confined system inhibits forward reactions, reducing the gas yield growth rate. Consequently, gas yield exhibits a trend of initial increase followed by decrease. The increase in gas yield does not entirely determine the oil/gas production efficiency of oil-rich coal samples; analysis of specific component contents in the produced gases remains essential. As

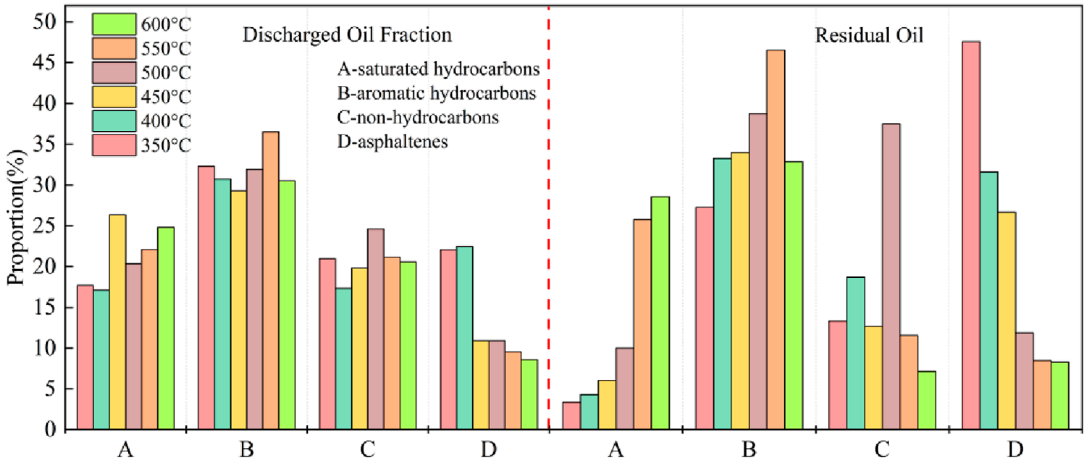

FIGURE 10
Comparison of residual and discharged oil fraction components.

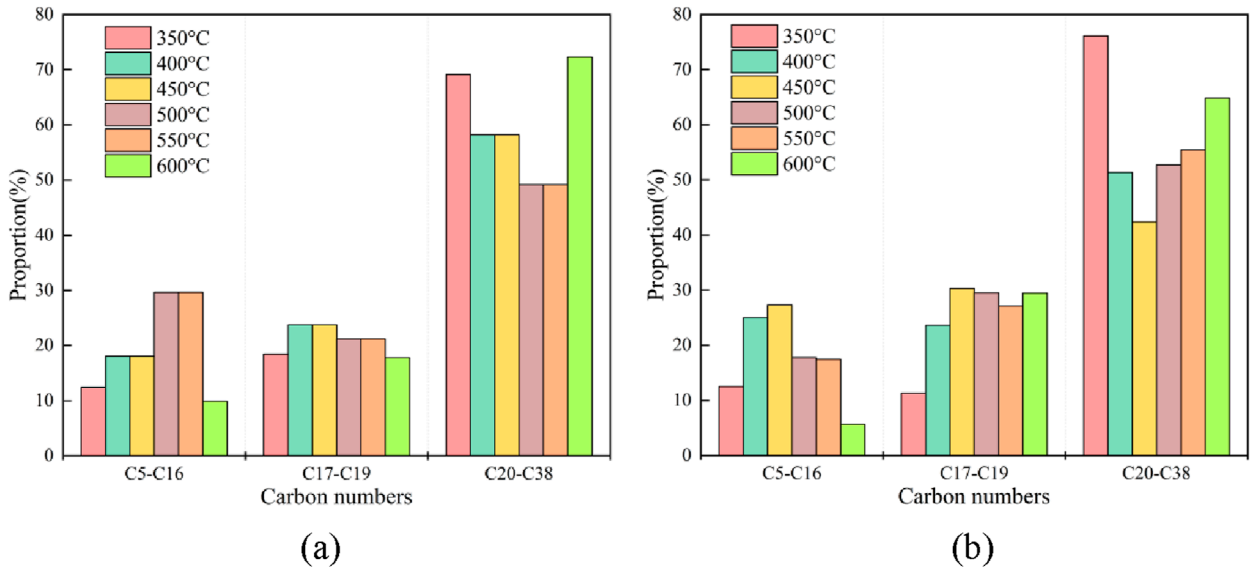

FIGURE 11
Carbon number distribution of pyrolysis residual oil and discharged oil. **(a)** Discharged oil. **(b)** Residual oil.

system temperature rises, the generation rates and proportions of different gas types exhibit significant variations: during low-temperature stages, pyrolysis reactions primarily involve cleavage of oxygen-containing functional groups like carboxyl and carbonyl groups, reactions accompanied by substantial CO_2 production, this was confirmed in the work of Li et al. (2018). making CO_2 the dominant gas component. With continued temperature increase, oxygen-containing functional groups gradually deplete, slowing CO_2 generation. At this stage, cleavage of multiple functional groups coupled with prolonged high-temperature reactions triggers secondary reactions in organic matter, generating abundant CH_4. Consequently, CO_2 proportion rapidly declines while CH_4 proportion surges. Upon further temperature rise, partial CH_4 participates in secondary cracking reactions of tar within oil-rich coal, causing a minor rebound in CO_2 and a corresponding decrease in CH_4 proportion. C_2 and C_3 gases, as primary products from thermal cleavage of macromolecular structures like aliphatic alkyl side chains and bridging bonds in oil-rich coal, have their proportions mainly governed by macromolecular pyrolysis (Xu et al., 2025). This reaction process intensifies most severely within the 350 °C–400 °C range. Within this interval, rising temperature accelerates aliphatic structure fragmentation, increasing C_2 and C_3 generation. However, further temperature elevation causes C_2 and C_3 gases to crack into CH_4 and semi-coke, thus reducing C_2/C_3 proportions while elevating CH_4 proportion. When heating oil-rich coal to 600 °C, pyrolysis enters the semi-coke

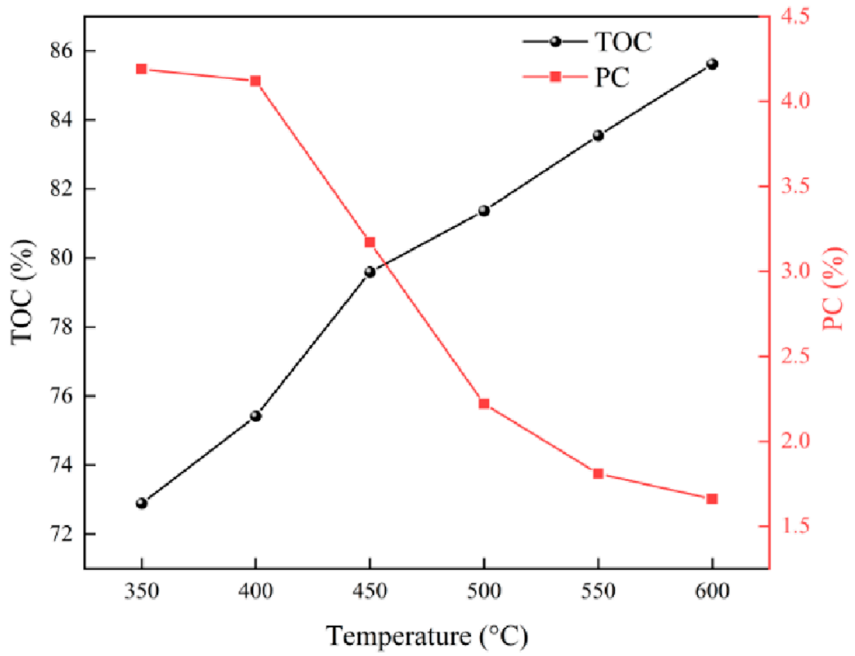

FIGURE 12
TOC and PC changes in Xiegou tar-rich coal pyrolysis residue with temperature.

polycondensation stage where tar cracking completes (Wang et al., 2024d; Fu et al., 2023b). Dehydrogenation during polycondensation becomes dominant, producing H_2. Additionally, since aliphatic fragmentation and aromatic sidechain cleavage primarily generate hydrocarbon gases and H_2 (Wang et al., 2024e), CO shows no significant upward trend. Comprehensive analysis of gas component yields confirms that 550 °C–600 °C constitutes a critical phase for *in-situ* pyrolysis of lump oil-rich coal, characterized by rising CH_4 and H_2 yields, establishing it as the optimal temperature window for natural gas extraction.

Secondly, for liquid products: during lower temperature stages, organic matter in oil-rich coal undergoes incomplete decomposition (Zhou et al., 2018), producing predominantly higher molecular-weight oils, thus liquid products are dominated by residual oil. When temperature rises to 450 °C, macromolecular organics undergo cracking reactions releasing light oil components, causing discharged oil yield to increase gradually. With the completion of organic cracking reactions and further temperature elevation, secondary reactions of pyrolytic oils generate substantial gases (Xu et al., 2019) while reducing both discharged and residual oil yields–corresponding to the characteristics of pyrolytic gaseous products. Specific analysis of the components in the liquid phase products reveals that, as saturated hydrocarbons primarily originate from the cracking of aliphatic structures (Yang et al., 2023a), the cracking of aliphatic structures intensifies with increasing temperature; the aromatic hydrocarbon component is markedly more pronouncedly affected by temperature, which is due to the fact that aromatic hydrocarbons mainly originate from the cleavage of aromatic side chains and aromatic condensation reactions, and the natural content of aromatics in oil-rich coal is inherently high (Yu et al., 2023), with increasing temperature the cleavage of aromatic side chains and aromatic condensation reactions generate more aromatic oils, and this reaction is more intense in the residual oil; Furthermore, as asphaltenes primarily originate from the condensation reactions of large molecular organic compounds, the temperature range of 400 °C–500 °C promotes the rapid progression of this reaction and accelerates the cracking of asphaltenes into light oils or gases, therefore their content decreases more significantly within this interval; total hydrocarbon chromatographic analysis of the liquid phase products reveals that, as light oil components primarily originate from the cracking of aliphatic structures, with increasing temperature the cracking of aliphatic structures accelerates, generating more light components, while in the high-temperature range, due to prolonged sealed pyrolysis, partial components undergo secondary reactions, at this stage light components decompose, generating hydrocarbon gases, when the primary pyrolysis reaction of the oil-rich coal sample occurs, at this stage heavy components crack into light hydrocarbons through β-position bond scission reactions (Zhao et al., 2025), therefore the proportion of heavy oil decreases, and when the temperature rises to 600 °C, due to prolonged *in-situ* sealed pyrolysis reactions causing high-temperature recombination of small molecular radicals in the retained oil, combining to form large molecular asphaltenes, the heavy oil component increases again, at this stage the yields of both retained oil and discharged oil significantly decrease, substantial amounts of short-chain coal tar transform into hydrocarbon gases, while the heavy components, due to their better thermal stability, decompose more slowly, further promoting the increase in their proportion; comprehensive analysis can determine the temperature range of 450 °C–550 °C as the optimal temperature window for light oil recovery.

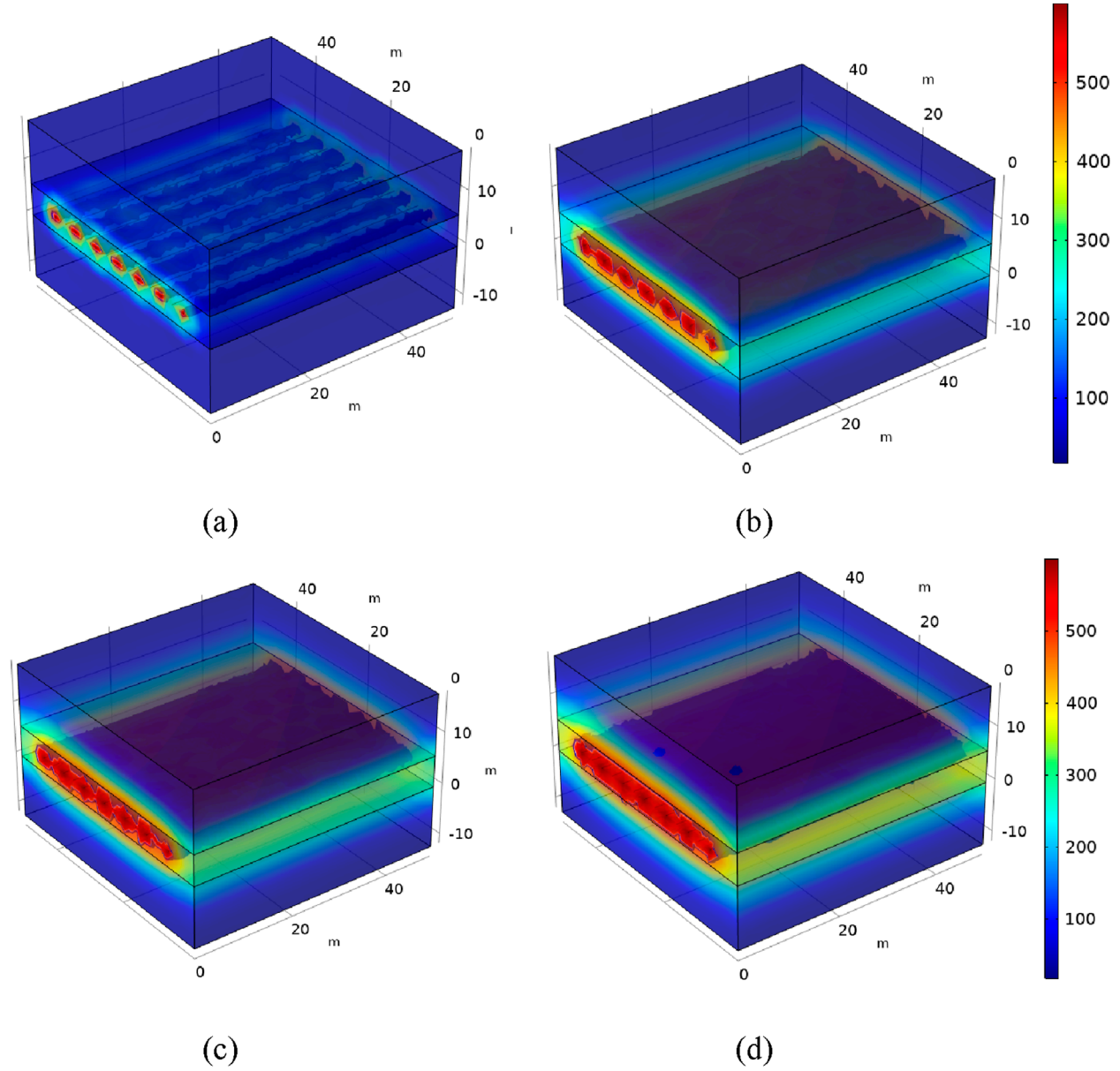

FIGURE 13
Temperature field distribution diagrams under different heating times. **(a)** 100 d. **(b)** 600 d. **(c)** 1,000 d. **(d)** 1,500 d.

Thirdly, the solid phase products from *in-situ* pyrolysis are primarily the solid residues generated after oil-gas separation, with increasing temperature the aliphatic side chains, oxygen-containing functional groups, and weak bonds in the coal sample fracture, generating small-molecule gases and tar which escape, resulting in a reduction in the total mass of the char and a gradual increase in the TOC proportion, simultaneously the PC content decreases; furthermore with increasing temperature aliphatic carbon transforms into more stable aromatic structures through cyclization and dehydrogenation reactions (Wu and Zhang, 2019), forming graphitic microcrystals, enhancing the stability of the carbon skeleton, while after high-temperature pyrolysis the inorganic carbon further decomposes causing the TOC content to rise; when the temperature is raised to 400 °C, due to the aliphatic structures fracturing to generate tar and pyrolysis gas, PC participates as a reaction intermediate in radical recombination, therefore its content exhibits significant changes at 350 °C.

Through industrial scale simulation of the oil and gas production from oil-rich coal, the effects in practical engineering applications can be effectively simulated, and the optimal time and temperature for oil and gas production can be sought; according to the simulation results, the peak CH_4 production from oil-rich coal pyrolysis occurs at 1,100 d, which is due to the fact that at this time the surface area of the high-temperature zone is the largest, after 1,100 d the pyrolysis of the oil-rich coal reservoir between the heaters is completed, and the growth rate of the high-temperature zone surface area slows down; this indicates that hydrogen generation requires high temperature for promotion, and its active period is short, the reason is similar to

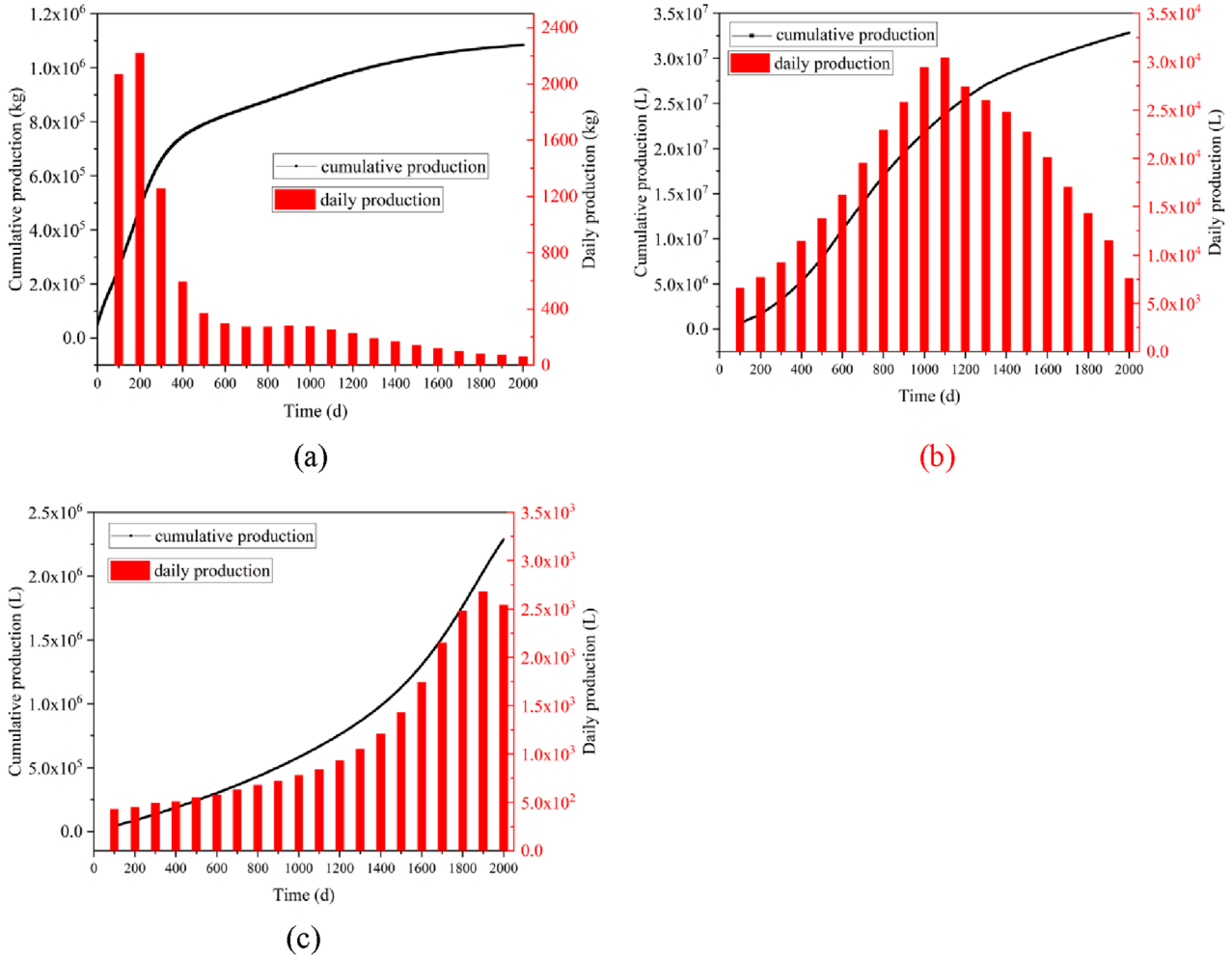

FIGURE 14
Variation patterns of major pyrolytic products over time. **(A)** Discharged oil. **(B)** CH_4. **(C)** H_2.

that of CH_4, both being related to the propagation of the temperature field, which is consistent with the law obtained from the previous experimental findings, reflecting the characteristic that methane is continuously generated during the middle stage of pyrolysis and ultimately reaches its peak.

Overall, the yields of the three-phase products align with the experimental results, and prolonged sealed experiments can effectively simulate the underground *in-situ* pyrolysis environment; therefore, for practical applications aimed at oil production, it is recommended that the heating time be controlled within 500 days; while during long-term production processes, the gaseous products will become predominant, thus prolnged pyrolysis is beneficial for development and utilization targeting natural gas.

5 Conclusion

Through systematic analysis of the pyrolysis behavior of Xiegou oil-rich coal under long-term reaction at different temperatures, this study reveals the distribution laws and reaction mechanisms of pyrolysis products. The main conclusions are as follows:

1. Total pyrolytic gas yield increases significantly with temperature, with CH_4 being the dominant component. CH_4 proportion peaks at 550 °C while its yield peaks at 600 °C, establishing 550 °C–600 °C as the optimal temperature window for natural gas extraction.
2. For liquid pyrolysis products: discharged oil yield peaks at 450 °C, while residual oil yield decreases monotonically with temperature. Within the 450 °C–550 °C interval, discharged oil exhibits high saturates content, indicating this range as the potential temperature window for maximizing light oil recovery.
3. In solid pyrolysis products: TOC increases and PC decreases with rising temperature, demonstrating enhanced carbon skeleton stability of oil-rich coal during pyrolysis, facilitating oil/gas extraction and utilization.
4. Industrial scale simulations recommend a 500 days heating period for optimal oil production, extending to 1,900 days for optimal gas production.

This study provides a theoretical basis for the development of *in-situ* pyrolysis technology for oil-rich coal and is of great significance for promoting the efficient development of coal-based oil and gas resources.

Data availability statement

The original contributions presented in the study are included in the article/supplementary material, further inquiries can be directed to the corresponding author.

Author contributions

XL: Writing – original draft, Writing – review and editing. YT: Conceptualization, Writing – original draft. YL: Investigation, Writing – review and editing. FY: Software, Writing – review and editing. XW: Data curation, Writing – review and editing. JS: Data curation, Writing – review and editing. JC: Methodology, Writing – review and editing. QZ: Formal Analysis, Writing – review and editing. SY: Formal Analysis, Writing – review and editing. ZK: Supervision, Writing – review and editing.

Funding

The author(s) declare that financial support was received for the research and/or publication of this article. The Open Fund Project of CNOOC Key Laboratory of Liquefied Natural Gas and Low-Carbon Technology (KJQZ-2024-1105).

Conflict of interest

The authors declare that the research was conducted in the absence of any commercial or financial relationships that could be construed as a potential conflict of interest.

Generative AI statement

The author(s) declare that no Generative AI was used in the creation of this manuscript.

Any alternative text (alt text) provided alongside figures in this article has been generated by Frontiers with the support of artificial intelligence and reasonable efforts have been made to ensure accuracy, including review by the authors wherever possible. If you identify any issues, please contact us.

Publisher's note

References

Bhattacharyya, M., Shadangi, K. P., Purkayastha, R., Mahanta, P., and Mohanty, K. (2024). Co-pyrolysis of coal and biomass blends: impact of pyrolysis temperature and biomass blending on thermal stability of coal, and composition of pyrolysis products. *Process Saf. Environ. Prot.* 187, 1010–1021. doi:10.1016/j.psep.2024.05.037

Chen, H., Chen, Y., and Kou, J. (2024). Energy stable finite element approximations of gas flow in poroelastic media. *Comput. Methods Appl. Mech. Eng.* 428. doi:10.1016/j.cma.2024.117082

Chen, M., Wang, C., Yuan, T., Ning, X., Huang, X., Deng, L., et al. (2025a). Experimental investigation on gas-liquid–solid tri-phase product distributions during the simulated *in-situ* pyrolysis of tar-rich coal. *Fuel* 381, 133465. doi:10.1016/j.fuel.2024.133465

Chen, Z., Song, S., Zhang, W., and Mei, S. (2025b). Investigation of thermal-hydraulic-mechanical coupling model for *in-situ* transformation of oil shale considering pore structure and anisotropy. *Eng. Geol.* 344, 107859. doi:10.1016/j.enggeo.2024.107859

Dong, Z., Chen, Y., and Zhang, M. (2025). Production capacity prediction of U-shaped horizontal wells for *in-situ* pyrolysis of tar-rich coal: experimental and numerical simulation study. *J. China Coal Soc.* 50 (2), 1175–1191. doi:10.13225/j.cnki.jccs.2024.0340

Duan, Z., Wang, F., and Wang, Z. (2024). Pilot experiment for underground *in-situ* pyrolysis of tar-rich coal in the northern Shaanxi Province. *Coal Geol. Explor.* 52 (7), 14–24. doi:10.12363/issn.1001-1986.24.05.0362

Feng, Z., Zhou, D., Zhao, Y., and Cai, T. (2016). Study on microstructural changes of coal after methane adsorption. *J. Nat. Gas. Sci. Eng.* 30, 28–37. doi:10.1016/j.jngse.2016.01.044

Fu, D., Duan, Z., and Yang, F. (2023a). Key problems in *in-situ* pyrolysis of tar-rich coal drilling for extraction of coal-based oil and gas resources. *J. China Coal Soc.* 48 (4), 1759–1772. doi:10.13225/j.cnki.jccs.2022.0183

Fu, D., Yu, Z., Gao, K., Duan, Z., Wang, Z., Guo, W., et al. (2023b). Thermodynamic analysis on *in situ* underground pyrolysis of tar-rich coal: secondary reactions. *ACS Omega* 8 (14), 12805–12819. doi:10.1021/acsomega.2c08033

Guo, W., Li, Q., Deng, S. H., Wang, Y., and Zhu, C. F. (2023). Mechanism and reservoir simulation study of the autothermic pyrolysis *in-situ* conversion process for oil shale recovery. *Pet. Sci.* 20 (2), 1053–1067. doi:10.1016/j.petsci.2022.08.030

Ju, Y., Zhu, Y., Zhou, H. W., and Xie, H. (2021). Microwave pyrolysis and its applications to the *in situ* recovery and conversion of oil from tar-rich coal: an overview on fundamentals, methods, and challenges. *Energy Rep.* 7, 523–536. doi:10.1016/j.egyr.2021.01.021

Ju, Y., Zhu, Y., and Zhang, Y. (2022). Effects of high-power microwave irradiation on tar-rich coal for realising *in situ* pyrolysis, fragmentation, and low-carbon utilisation of tar-rich coal. *Int. J. Rock Mech. Min. Sci.*, 157. doi:10.1016/j.ijrmms.2022.105165

Kang, Z., Zhao, Y., and Yang, D. (2020). Review of oil shale *in-situ* conversion technology. *Appl. Energy* 269, 115121. doi:10.1016/j.apenergy.2020.115121

Kou, J., Wang, X., Chen, H., and Sun, S. (2023). An energy stable, conservative and bounds-preserving numerical method for thermodynamically consistent modeling of incompressible two-phase flow in porous media with rock compressibility. *Int. J. Numer. Meth Eng.* 124 (11), 2589–2617. doi:10.1002/nme.7222

Krumm, R. L., Gneshin, K. W., and Deo, M. (2017). Adsorption characteristics of coals pyrolyzed at slow heating rates. *Energy Fuels* 31 (2), 1803–1810. doi:10.1021/acs.energyfuels.6b03116

Li, J., Li, Z., Yang, Y., and Wang, C. (2018). Study on oxidation and gas release of active sites after low-temperature pyrolysis of coal. *Fuel* 233, 237–246. doi:10.1016/j.fuel.2018.06.039

Ning, X., Huang, X., Xue, X., Wang, C., Deng, L., and Che, D. (2025). Experimental study on yield and quality of tar from tar-rich coal under the simulated *in-situ* conditions. *J. Energy Inst.* 118, 101912. doi:10.1016/j.joei.2024.101912

Tian, H., Zhang, R., and Wang, Q. (2024). Spatiotemporal distributions of typical contaminants from the *in-situ* pyrolysis of tar-rich coals. *Coal Geol. Explor*. 52 (7), 64–72. doi:10.12363/issn.1001-1986.24.01.0052

Wang, X., and Feng, Z. (2021). Thermal deformation of long flame coal under thermo-mechanical coupling. *Coal Eng.* 53 (06). doi:10.11799/ce202106026

Wang, G., Yang, D., Kang, Z., Zhao, J., and Lv, Y. (2019). Numerical investigation of the *in situ* oil shale pyrolysis process by superheated steam considering the anisotropy of the thermal, hydraulic, and mechanical characteristics of oil shale. *Energy and Fuels* 33 (12), 12236–12250. doi:10.1021/acs.energyfuels.9b02883

Wang, S., Shi, Q., and Wang, S. (2021). Resource property and exploitation concepts with green and low-carbon of tar-rich coal as coal-based oil and gas. *J. China Coal Soc.* 46 (5), 1365–1377. doi:10.13225/j.cnki.jccs.ST21.0860

Wang, S., Shi, Q., and Sun, Q. (2024a). Strategic value and scientific exploration of *in-situ* pyrolysis of tar-rich coals. *Coal Geol. Explor.* 52 (7), 1–13. doi:10.12363/issn.1001-1986.24.06.0412

Wang, M., Wang, C., and Ning, X. (2024b). Research progress of *in-situ* pyrolysis technology for tar-rich coal. *J. China Coal Soc.* 49 (9), 3969–3984. doi:10.13225/j.cnki.jccs.2023.0790

Wang, L., Zhang, R., Zhao, J., Yang, D., Kang, Z., et al. (2024c). Effect of long reaction distance on gas composition from organic-rich shale pyrolysis under high-temperature steam environment. *Int. J. Coal Sci. and Technol.* 11 (1), 34. doi:10.1007/s40789-024-00689-7

Wang, K., Guo, L., Zhai, X., Deng, J., and Li, Y. (2024d). Hydrogen abstraction reaction mechanism of oil-rich coal spontaneous combustion. *Fuel* 367, 131538. doi:10.1016/j.fuel.2024.131538

Wang, K., Ding, J., Deng, J., Zhai, X., and Zhang, Y. (2024e). Hydrogen generation mechanism of oil-rich coal oxidation in low temperature. *Energy* 293, 130739. doi:10.1016/j.energy.2024.130739

Wang, L., Wang, G., Yang, D., Zhao, J., Kang, Z., Zeng, Q., et al. (2025a). Research on the mechanical properties and anisotropy evolution of uniaxial compression of oil shale under real-time high-temperature steam. *Rock Mech. Rock Eng.* 58 (2), 1911–1932. doi:10.1007/s00603-024-04246-1

Wang, L., Wang, Z., Zhao, Y., Zhang, R., Yang, D., Kang, Z., et al. (2025b). Macroscopic seepage and microstructural behavior of oil shale using water vapor injection during mining. *J. Rock Mech. Geotechnical Eng.* 17 (3), 1489–1509. doi:10.1016/j.jrmge.2024.10.024

Wu, D., and Zhang, W. (2019). Evolution mechanism of macromolecular structure in coal during heat treatment: based on FTIR and XRD *in situ* analysis techniques. *J. Spectrosc.* 2019, 1–18. doi:10.1155/2019/5037836

Wu, H., Chen, Y., Lv, H., Xie, Q., and Gu, J. (2022). Stability analysis of rib pillars in highwall mining under dynamic and static loads in open-pit coal mine. *Int. J. Coal Sci. Techn* 9 (1), 38. doi:10.1007/s40789-022-00504-1

Xie, X., Zhao, Y., Qiu, P., Lin, D., Qian, J., Hou, H., et al. (2018). Investigation of the relationship between infrared structure and pyrolysis reactivity of coals with different ranks. *Fuel* 216, 521–530. doi:10.1016/j.fuel.2017.12.049

Xu, F., Liu, H., Wang, Q., Pan, S., Zhao, D., Liu, Q., et al. (2019). ReaxFF-based molecular dynamics simulation of the initial pyrolysis mechanism of lignite. *Fuel Process. Technol.* 195, 106147. doi:10.1016/j.fuproc.2019.106147

Xu, T., Chen, L., Chen, J., Lei, Y., Wang, X., Yang, X., et al. (2025). Characteristics of pyrolysis products of tar-rich coal under cryogenic pretreatment with liquid nitrogen. *Processes* 13, 1064. doi:10.3390/pr13041064

Yang, D., Wang, L., Zhao, Y., and Kang, Z. (2021). Investigating pilot test of oil shale pyrolysis and oil and gas upgrading by water vapor injection. *J. Pet. Sci. Eng.* 196, 108101. doi:10.1016/j.petrol.2020.108101

Yang, F., Gao, K., Yu, Z., Ma, L., Cao, H., Yang, P., et al. (2023a). Thermodynamic analysis of *in situ* underground pyrolysis of tar-rich coal: primary reactions. *Acs Omega* 8 (21), 18915–18929. doi:10.1021/acsomega.3c01321

Yang, F., Cheng, X., Li, M., Wei, J., Duan, Z., and Ma, L. (2023b). Numerical investigation of the heat and mass transfer during the *in situ* pyrolysis process of oil-rich coal. *Processes* 11 (11), 3226. doi:10.3390/pr11113226

Ye, Q., Li, M., Hao, J., Huang, Z., and Wei, J. (2023). Multi-physics simulation of tar-rich coal *in situ* pyrolysis with a multiregion homogenization treatment. *ACS Omega* 8 (36), 32565–32579. doi:10.1021/acsomega.3c01481

Yu, Z., Guo, W., Yang, P., Zhang, J., Gao, K., Shang, J., et al. (2023). *In-situ* infrared and kinetic characteristics analysis on pyrolysis of tar-rich coal and macerals. *Fuel* 348, 128601. doi:10.1016/j.fuel.2023.128601

Yu, G., Bai, X., Fan, X., He, X. Y., Zou, H. X., Dilixiati, Y., et al. (2024a). *In-situ* evaluation of volatile products released during pyrolysis of coals with different ranks. *J. Energy Inst.* 115, 101660. doi:10.1016/j.joei.2024.101660

Yu, Z., Guo, W., Yang, P., Yang, F., Ma, L., Wang, J., et al. (2024b). Kinetic characteristics and product distribution of tar-rich coal *in-situ* underground pyrolysis: influence of heterogeneous coal seam. *J. Anal. Appl. Pyrolysis.* 183, 106729. doi:10.1016/j.jaap.2024.106729

Yuan, T., Wang, C. A., Chen, M., Yang, F., Hou, Y., Ma, L., et al. (2025). Simulation investigation on separation characteristics of gas-liquid model products from *in-situ* pyrolysis of tar-rich coal. *J. Environ. Chem. Eng.* 13 (2), 115719. doi:10.1016/j.jece.2025.115719

Zhang, Z., Zhou, A., Shi, Z., Zhang, H., He, X., Wang, Y., et al. (2025). Explaining relationships between chemical structure and tar-rich coal pyrolysis products yield based on pearson correlation coefficient. *Fuel* 395, 135029. doi:10.1016/j.fuel.2025.135029

Zhao, J., Shi, Q., and Wang, S. (2025). Study on molecular structural heterogeneity of tar-rich coal based on micro-FTIR. *Spectrochim. Acta A*, 330. doi:10.1016/j.saa.2025.125749

Zhou, G., Zhong, W., Yu, A., Dou, Y., and Yin, J. (2018). Experimental study on characteristics of pressurized grade conversion of coal. *Fuel* 234, 965–973. doi:10.1016/j.fuel.2018.07.142